# Fluctuations and noise signatures of driven magnetic skyrmions

Sebastián A. Díaz, C. J. O. Reichhardt, Daniel P. Arovas, Avadh Saxena, and C. Reichhardt

# Fluctuations and Noise Signatures of Driven Magnetic Skyrmions

Sebastián A. Díaz,[1,2] C.J.O. Reichhardt,[1] Daniel P. Arovas,[2] Avadh Saxena,[1] and C. Reichhardt[1]

[1] *Theoretical Division and Center for Nonlinear Studies,*
*Los Alamos National Laboratory, Los Alamos, New Mexico 87545, USA*
[2] *Department of Physics, University of California, San Diego, La Jolla, California 92093, USA*

Magnetic skyrmions are particle-like objects with topologically-protected stability which can be set into motion with an applied current. Using a particle-based model we simulate current-driven magnetic skyrmions interacting with random quenched disorder and examine the skyrmion velocity fluctuations parallel and perpendicular to the direction of motion as a function of increasing drive. We show that the Magnus force contribution to skyrmion dynamics combined with the random pinning produces an isotropic effective shaking temperature. As a result, the skyrmions form a moving crystal at large drives instead of the moving smectic state observed in systems with a negligible Magnus force where the effective shaking temperature is anisotropic. We demonstrate that spectral analysis of the velocity noise fluctuations can be used to identify dynamical phase transitions and to extract information about the different dynamic phases, and show how the velocity noise fluctuations are correlated with changes in the skyrmion Hall angle, transport features, and skyrmion lattice structure.

## I. INTRODUCTION

Skyrmions are particle-like objects that emerge due to collective interactions of atomic-scale magnetic degrees of freedom, and they are stabilized by their topological properties[1–3]. An increasing number of magnetic systems capable of supporting skyrmions have been identified, including recent work on materials in which the skyrmions are stable at room temperature[4–7]. Skyrmions can also be readily set into motion with an applied current[8–16], and this property, along with their size scale, makes them promising candidates as information carriers for applications in high-density magnetic storage[17–20] and novel logic devices[21,22].

Similar to other particle-like objects such as vortices in type-II superconductors[23–26], electrons in Wigner crystals[27–29], and colloids moving on a rough substrate[30–32], skyrmions exhibit depinning and collective dynamics when driven over quenched disorder[33]. All of these systems can exhibit dynamical transitions between distinct types of motion as a function of the strength of the driving force. Such dynamic phases include a low drive pinned phase, a plastic or disordered flow phase in which there is a combination of moving and pinned particles[23,30,31,33–35], moving liquid phases in which all the particles are in motion but the overall moving structure is disordered[23,33], and high driving dynamically ordered or quasi-ordered states including moving smectic states and moving anisotropic crystals[23,25,26,28,32,33,36–43]. These different phases can be identified by direct visualization[39,41], changes in the structure factor of the particle configurations[25,37,38,40,42,43] and features in the transport curves or differential conductivity[23,26,28,33,34,36,38,40]. The dynamic states can also be characterized by measuring changes in the noise fluctuations of the moving particles as a function of increasing drive[33]. One of the best examples of a system in which noise fluctuations can be used to identify the dynamical states is flux motion in type-II superconductors, where the voltage noise generated at fixed current or drive is produced by the velocity fluctuations of the vortices. Both experiments and simulations show that in the plastic flow regime the noise fluctuations typically exhibit a large low frequency component with a $1/f^\alpha$ characteristic[24,38,43] where $\alpha = 1.0$ to 2.0, while in the moving liquid phase the noise is white with $\alpha = 0$[24,38]. At higher drives when a moving ordered state forms, a narrow band noise signature appears with peaks at frequencies that are correlated with the periodicity of the moving structure[38,41,43–46].

Koshelev and Vinokur[36] argued that the transition from the disordered flow state to the ordered flow state at higher drives in vortex systems can be understood by representing the fluctuating forces exerted by the pinning sites on the moving vortices as an effective shaking temperature $T_{sh}$. As the driving force $F_d$ increases, $T_{sh}$ decreases according to $T_{sh} \sim 1/F_d$ since the more rapidly moving vortices have less time to respond to the pinning forces. At high drives the pinning sites act only as a weak perturbation of magnitude $T_{sh}$ on the rapidly moving vortices, and the mutual repulsion between vortices dominates over the pinning forces so that the vortices form an ordered lattice. In contrast, at lower drives the fluctuations created by the pinning sites are stronger and $T_{sh}$ becomes large enough to melt the vortex lattice, in analogy to the melting of an equilibrium system under ordinary thermal fluctuations. Further theoretical work[47,48] showed that due to the direction of the external driving force, the shaking temperature from the pinning-induced dynamical perturbations is anisotropic, and thus the dynamically ordered state is also anisotropic, taking the form of a moving smectic or a moving anisotropic crystal. Such states have been observed in experiment[39] and simulations[37,38,40]. Computational studies have also directly shown that the dynamic fluctuations in the different phases are anisotropic[40] and that the shaking tem-

perature decreases with increasing drive[49].

Skyrmions share many features with vortices in type-II superconductors. Both are particle-like objects with repulsive interactions, both form triangular lattices in the absence of quenched disorder, and both can be set into motion with an applied current. Thus, analyzing the noise fluctuations of moving skyrmions should provide a valuable method for characterizing the skyrmion dynamics. One key difference between vortices and skyrmions is that skyrmion motion typically has a large Magnus component, while vortex systems are generally in the overdamped limit where the Magnus term is weak or absent. The Magnus term generates a skyrmion velocity component that is perpendicular to the external force, and it is not known what effect this has on the noise fluctuations. Due to the Magnus term, the skyrmions move at an angle, called the skyrmion Hall angle $\theta_{Sk}$, with respect to the driving force. In the absence of pinning $\theta_{Sk}$ has a fixed intrinsic value of $\theta_{Sk}^{int} = \arctan(\alpha_m/\alpha_d)$ where $\alpha_m$ is the strength of the Magnus term and $\alpha_d$ is the damping coefficient. Both simulations[16,50–54] and experiments[14,15] have shown that when pinning is present, $\theta_{Sk}$ is strongly drive dependent, taking the value $\theta_{Sk} \approx 0$ just above depinning and increasing to $\theta_{Sk} \approx \theta_{Sk}^{int}$ at high drives where the dynamic fluctuations induced by the pinning are reduced. This drive dependence is a result of the side-jump motions the skyrmions experience when they interact with pinning sites, which diminishes at higher drives[50–52,55]. Previous simulation work showed that in the presence of pinning the skyrmions form a pinned skyrmion glass that depins plastically into a disordered flowing state followed by a transition to an ordered flowing state at high drives[51]. Unlike the overdamped vortices, which form a moving smectic state, the skyrmions form a moving isotropic crystal, suggesting that the dynamic fluctuations and shaking temperature experienced by the moving skyrmions are different in nature from those in the vortex system. Previous numerical studies indicate that skyrmions show a broad band noise signature near depinning and narrow band noise at high drives[53]; however, these studies were limited in scope and did not include diffusive measures that could indicate how the fluctuations correlate with the structure of the moving skyrmions.

Here we examine skyrmions moving over random quenched disorder and measure the velocity fluctuations both parallel and perpendicular to the direction of skyrmion motion for varied intrinsic skyrmion Hall angles and drives. We use a particle-based model[16,50–53,55] in which the skyrmion dynamics is described by a modified Thiele equation[55,56]. In the overdamped limit the Hall angle is zero with respect to the driving direction, the velocity fluctuations are highly anisotropic at all drives, and the system forms a moving smectic state at large drives as indicated by the presence of two dominant peaks in the structure factor. When the Magnus term is finite, we find that the velocity fluctuations are anisotropic in the plastic flow regime but become isotropic at the transition

to a moving ordered phase in which the skyrmions form a moving triangular crystal with equal weight in the six Bragg peaks of the structure factor. The skyrmion Hall angle is zero just at depinning within the plastic flow regime and gradually increases with increasing drive before saturating to a value close to $\theta_{Sk}^{int}$ at the transition to the moving crystal state. We show that the velocity noise fluctuations undergo a crossover from a broad band noise signature in the plastic flow phase to narrow band noise in the moving crystal. In general the skyrmion system exhibits a richer variety of narrow band noise than the vortex system, such as switching events that are associated with small rotations in the moving lattice. We also show that at small but finite intrinsic skyrmion Hall angles, multiple dynamical transitions can occur in the moving state, including a transition from disordered flow to a moving smectic followed by a transition to a moving crystal. These transitions can be detected through changes in the velocity noise signal and jumps in the skyrmion Hall angle.

The paper is organized as follows. In Section II we describe the system and our simulation method. Section III covers the dynamic phases observed for varied intrinsic skyrmion Hall angles, the behavior of the velocity fluctuations parallel and perpendicular to the skyrmion motion, and the correlation of these fluctuations with changes in transport curves, particle structure, and $\theta_{Sk}$. In Section III A we show how the different dynamic phases produce distinct structure factor signatures, while in Section III B we examine the diffusive behavior in the moving frame and find that the shaking temperature in the dynamically ordered phase is generally isotropic for skyrmions and anisotropic in the overdamped limit. We consider the limit of small intrinsic skyrmion Hall angles in Section III C and show that the system exhibits both a moving smectic and a moving crystal phase. In Section IV we measure the velocity noise signals both parallel and perpendicular to the direction of skyrmion motion and show that there is a transition from broad band noise in the plastic flow region to a narrow band noise signal in the moving crystal state. We discuss possible future directions in Section V, and in Section VI we provide a summary of our results.

## II. MODEL AND SIMULATION

We consider a two-dimensional system in which the skyrmions are modeled as point particles obeying dynamics that are described by a modified Thiele's equation which includes quenched disorder and skyrmion-skyrmion interactions[55,56]. The particle-based model is applicable under conditions where excitation of internal modes in individual skyrmions can be neglected and where the distance between skyrmions is comparable to or larger than the size of an individual skyrmion. We simulate $N = 480$ skyrmions moving in a system of size $L_x \times L_y$ with $L_x = 34.64$ and $L_y = 36$ contain-

ing $N_p = 259$ randomly distributed pinning sites. The equation of motion of skyrmion $i$ is given by

$$\alpha_d \boldsymbol{v}_i - \alpha_m \hat{\boldsymbol{z}} \times \boldsymbol{v}_i = \boldsymbol{F}_i^{ss} + \boldsymbol{F}_i^p + \boldsymbol{F}^D. \qquad (1)$$

Here $\boldsymbol{v}_i = d\boldsymbol{r}_i/dt$ is the instantaneous velocity and $\boldsymbol{r}_i$ is the position of skyrmion $i$, while $\alpha_d = 1.0$ is the damping coefficient for the dissipative viscous force. The second term on the left hand side is the Magnus force which originates from the topological charge of each skyrmion. It produces no work and causes the skyrmions to move in the direction perpendicular to the net force. The skyrmion-skyrmion interaction force[51,55] is given by $\boldsymbol{F}_i^{ss} = \sum_{j=1}^{N} K_1(r_{ij}) \hat{\boldsymbol{r}}_{ij}$, where $r_{ij} = |\boldsymbol{r}_i - \boldsymbol{r}_j|$, $\hat{\boldsymbol{r}}_{ij} = (\boldsymbol{r}_i - \boldsymbol{r}_j)/r_{ij}$, and $K_1$ is the modified Bessel function of the second kind. The randomly distributed pinning sites are modeled as finite range parabolic traps that produce a pinning force described by $\boldsymbol{F}_i^p = \sum_{k=1}^{N_p} (F_p/r_p)(\boldsymbol{r}_i - \boldsymbol{r}_k^{(p)}) \Theta(r_p - |\boldsymbol{r}_i - \boldsymbol{r}_k^{(p)}|)$, where $F_p = 1.5$ is the maximum pinning force, $r_p = 0.35$ is the radius of the pinning sites, $\boldsymbol{r}_k^{(p)}$ is the location of the $k$-th pinning site, and $\Theta$ is the Heaviside step function. The external driving force, $\boldsymbol{F}^D = F_D \hat{\boldsymbol{x}}$, represents the Lorentz force exerted on the emergent quantized magnetic flux carried by each skyrmion by an applied electric current[3,9]. The dynamics of superconducting vortices are also described by Eq. (1) in the limit where the coefficient $\alpha_m$ of the Magnus term vanishes, since the vortex dynamics are dominated by damping. We refer to the case $\alpha_m = 0$ as the overdamped vortex limit.

We measure $\mathbf{V} = N^{-1} \sum_{i=1}^{N} \boldsymbol{v}_i$, the instantaneous velocity averaged over all of the skyrmions, as well as its time-averaged value $\langle \mathbf{V} \rangle$. In the absence of pinning sites, the angle $\theta$ between $\mathbf{V}$ and the driving force is equal to $\theta_{Sk}^{int}$, the intrinsic skyrmion Hall angle. When pinning is present, however, $\theta$ fluctuates around the drive-dependent value of $\theta_{Sk}$. We resolve $\mathbf{V}$ into components $V_{||} = \mathbf{V} \cdot \hat{\boldsymbol{x}} \cos\theta_{Sk} + \mathbf{V} \cdot \hat{\boldsymbol{y}} \sin\theta_{Sk}$ and $V_{\perp} = \mathbf{V} \cdot \hat{\boldsymbol{y}} \cos\theta_{Sk} - \mathbf{V} \cdot \hat{\boldsymbol{x}} \sin\theta_{Sk}$ that are parallel and perpendicular, respectively, to the direction of $\theta_{Sk}$. Figure 1 shows an image of our system as well as a diagram illustrating the relationship between $\mathbf{V}$, $V_{||}$, $V_{\perp}$, $\theta_{Sk}$, and the driving force $F_D$ which is applied along the $x$ direction.

To investigate the effect of the Magnus term, we perform simulations for different values of $\alpha_m$ corresponding to intrinsic skyrmion Hall angles of $\theta_{Sk}^{int} = 0°, 10°, 20°, 30°, 45°, 60°, 70°,$ and $80°$. We initialize the skyrmions in a triangular lattice and slowly increase $F_D$ from $F_D = 0$ to $F_D = 8.0$ in increments of $\Delta F_D = 0.01$ every $5 \times 10^5$ simulation time steps. For each drive increment, we allow the system to equilibrate during $5 \times 10^4$ simulation time steps, compute $\theta_{Sk}$ for the equilibrated system based on the direction of $\langle \mathbf{V} \rangle$, and then use $\theta_{Sk}$ to measure $V_{||}$ and $V_{\perp}$ during the remaining $4.5 \times 10^5$ simulation time steps. From the resulting time series we construct $\sigma_{||}$ and $\sigma_{\perp}$, the standard deviations of $V_{||}$ and $V_{\perp}$, respectively. We also obtain $S_{||}(\omega)$ and $S_{\perp}(\omega)$, the power spectral densities of the fluctuations in the parallel and
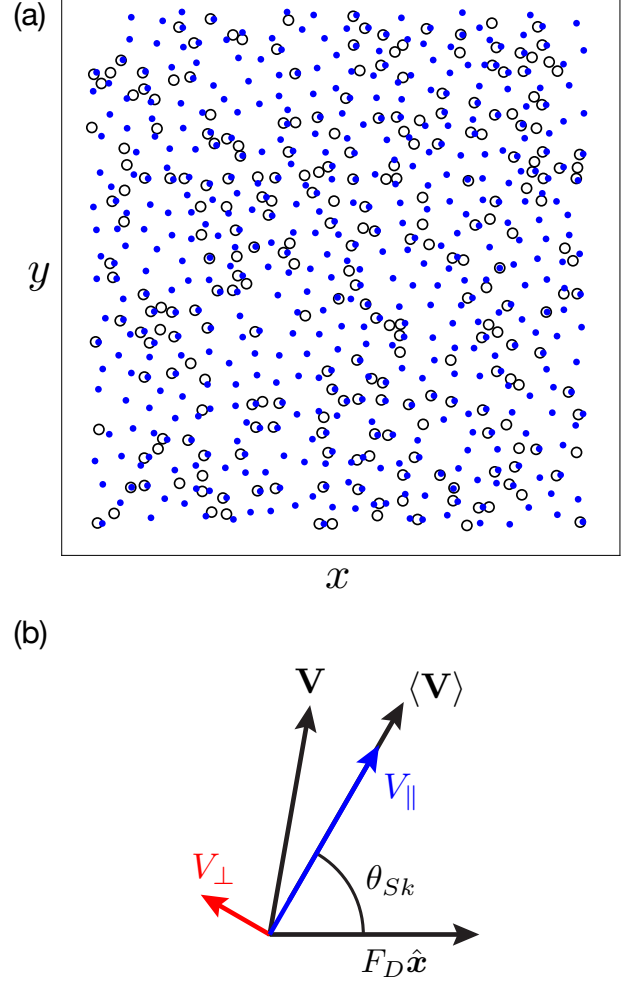


FIG. 1. (a) Real-space snapshot of the simulated system. Open black circles indicate pinning sites and filled blue dots indicate the instantaneous skyrmion positions. (b) Diagram illustrating the relationship between the driving force $F_D \hat{\boldsymbol{x}}$ applied along the $x$ direction and the instantaneous skyrmion velocity $\mathbf{V}$ averaged over all skyrmions. The skyrmion Hall angle $\theta_{Sk}$ varies with $F_D$, and the time-averaged skyrmion velocity $\langle \mathbf{V} \rangle$ is aligned with $\theta_{Sk}$. The direction of $\mathbf{V}$ fluctuates around $\theta_{Sk}$ and we resolve $\mathbf{V}$ into its components $V_{||}$ and $V_{\perp}$ that are parallel and perpendicular, respectively, to the direction defined by $\theta_{Sk}$.

perpendicular velocity components. Using the instantaneous positions of all the skyrmions, we calculate the mean squared displacements $\Delta_{||}$ and $\Delta_{\perp}$ parallel and perpendicular to $\langle \mathbf{V} \rangle$, as well as the static structure factor $S(\boldsymbol{q}) = \left| N^{-1} \sum_{i=1}^{N} \exp\left[i\boldsymbol{q} \cdot \boldsymbol{r}_i\right] \right|^2$. We determine $P_n$, the fraction of $n$-fold coordinated skyrmions, according to $P_n = N^{-1} \sum_{i=1}^{N} \delta(n - z_i)$ where $z_i$ is the coordination number of skyrmion $i$ obtained from a Voronoi tessellation. We focus on $P_6$, which measures the amount of six-fold or hexagonal ordering of the moving skyrmions, as well as $P_5$ and $P_7$, which are correlated with the appearance of dislocations composed of 5-7 paired dislocations.

There is also some finite weight in $P_4$ due to the shearing of a triangular lattice structure. All other coordination numbers have vanishing weight and are not shown.
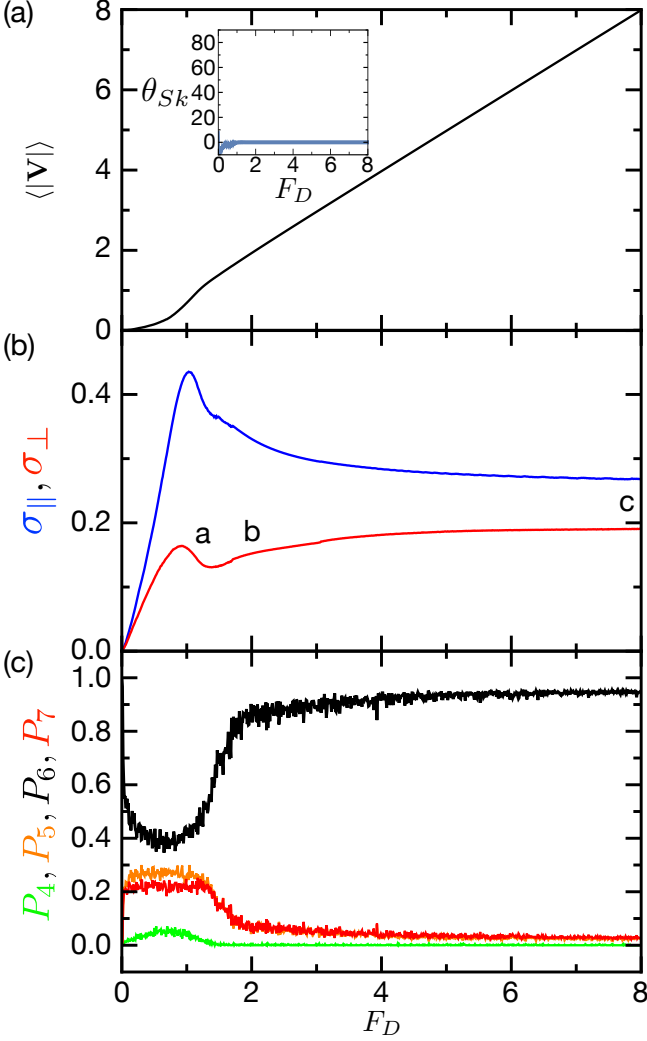
## III. DYNAMIC PHASES



FIG. 2. Results from the overdamped limit $\alpha_m = 0$ with $\theta_{Sk}^{int} = 0°$. (a) Magnitude of the time-averaged velocity $\langle|\mathbf{V}|\rangle$ vs driving force $F_D$. The inset shows $\theta_{Sk}$ vs $F_D$, where there is no driving force dependence and $\theta_{Sk} = 0°$. (b) Standard deviation $\sigma_{||}$ (upper blue curve) and $\sigma_\perp$ (lower red curve) of the parallel and perpendicular instantaneous velocity, respectively, vs $F_D$ showing a strong anisotropy. The labels a, b, and c indicate the values of $F_D$ at which the structure factors in Fig. 5(a,b,c) were obtained. (c) $P_4$ (lower green curve), $P_5$ (central light orange curve), $P_6$ (upper black curve), and $P_7$ (central dark red curve), the fraction of 4-, 5-, 6-, and 7-fold coordinated particles, respectively, vs $F_D$ showing a transition to an ordered state near $F_D = 2.0$.

In Fig. 2(a) we plot the magnitude of the time-averaged velocity $\langle|\mathbf{V}|\rangle$ versus driving force $F_D$ for the overdamped

vortex limit with $\alpha_m = 0$ and $\theta_{Sk}^{int} = 0$. For $F_D < 2.0$, $\langle|\mathbf{V}|\rangle$ has a nonlinear shape consistent with a plastic depinning process, and crosses over to a linear dependence on driving force for $F_D \geq 2.0$. As shown in the inset of Fig. 2(a), $\theta_{Sk} = 0$ for all $F_D$, indicating that the particles are moving in the direction of the applied drive, as expected for the vortex limit. In Fig. 2(b), the plot of $\sigma_{||}$ and $\sigma_\perp$ versus $F_D$ indicates that the velocity fluctuations are strongly anisotropic, with $\sigma_{||} > \sigma_\perp$. Both $\sigma_{||}$ and $\sigma_\perp$ reach peak values near $F_D = 1.0$, indicating a maximum in the plasticity of the flow. This is followed by a decrease in $\sigma_{||}$ to a saturation value of $\sigma_{||} \approx 0.27$ at high drives, and a dip in $\sigma_\perp$ followed by a gradual increase to a saturation value of $\sigma_\perp \approx 0.19$ at high drives. The plots of $P_4$, $P_5$, $P_6$, and $P_7$ versus $F_D$ in Fig 2(c) show that for $0.0 < F_D < 1.2$, $P_6 \approx 0.4$ and the vortex positions are strongly disordered. For $F_D > 1.2$, $P_6$ increases to a value of $P_6 \approx 0.9$ indicating that dynamical reordering of the vortices has occurred, while $P_5$ and $P_7$ drop to $P_{5,7} \approx 0.05$ and track each other as the defects form paired 5-7 gliding dislocations.

Figure 3 illustrates the same quantities as above in a system with a finite Magnus term where $\theta_{Sk}^{int} = 45°$. In Fig. 3(a), the shape of $\langle|\mathbf{V}|\rangle$ versus $F_D$ is nonlinear for $F_D < 2.0$, indicating a plastic depinning process similar to that of the $\theta_{Sk}^{int} = 0°$ case shown in Fig. 2(a), but with a lower overall magnitude of $\langle|\mathbf{V}|\rangle$. The plot of $\sigma_{||}$ and $\sigma_\perp$ versus $F_D$ in Fig. 3(b) shows that $\sigma_{||} > \sigma_\perp$ only for $F_D < 2.5$ in the disordered flow regime, while for $F_D \geq 2.5$ when the system has dynamically ordered, $\sigma_{||} \approx \sigma_\perp$, indicating that the velocity fluctuations are isotropic unlike in the vortex case. In Fig. 3(c), we plot $P_4$, $P_5$, $P_6$, and $P_7$ versus $F_D$. The disordered plastic flow with low $P_6$ and high $\sigma_{||}$ persists out to slightly higher drives in the $\theta_{Sk}^{int} = 45°$ system compared to the vortex system, as indicated by the fact that the peak in $\sigma_{||}$ occurs at $F_D = 1.1$ in Fig. 3(b) but at $F_D = 1.0$ in Fig. 2(b). The dynamic reordering also shifts to higher drives, falling at $F_D = 2.0$ in Fig. 2(c) but at $F_D = 2.5$ in Fig. 3(c); however, although $P_6$ continues to slowly increase with $F_D$ in the vortex system above the dynamic reordering transition, in the $\theta_{Sk}^{int} = 45°$ system $P_6$ reaches a higher saturation value of $P_6 = 0.96$ at $F_D = 2.5$ and does not evolve as $F_D$ further increases, as shown in the inset of Fig. 3(c). This difference is due to the anisotropic velocity fluctuations in the vortex case, where the dislocations remaining after the dynamic reordering process has occurred undergo gliding motion and can only slowly annihilate each other, and the isotropic velocity fluctuations in the skyrmion case, where the remaining dislocations can climb under effectively thermal excitations and annihilate each other much more efficiently. The inset of Fig. 3(a) shows that $\theta_{Sk} \approx 0$ at small $F_D$ and gradually increases to $\theta_{Sk} = \theta_{Sk}^{int} = 45°$, reaching its saturation value at $F_D = 1.5$ where the difference between $\sigma_{||}$ and $\sigma_\perp$ in Fig. 3(b) has become small. This indicates that the direction of skyrmion motion in the plastic flow state gradually rotates until the drive is high enough that all
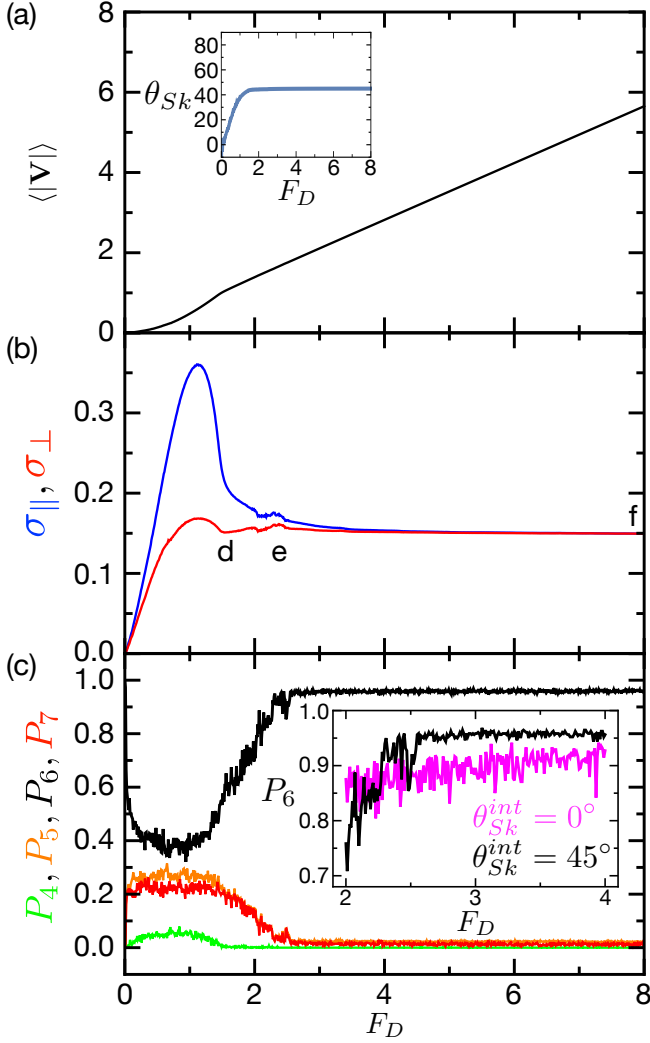
FIG. 3. Results from a system with $\theta_{Sk}^{int} = 45°$. (a) $\langle|\mathbf{V}|\rangle$ vs $F_D$. The inset shows $\theta_{Sk}$ vs $F_D$ where $\theta_{Sk} = 0°$ at $F_D = 0$ and increases to $\theta_{Sk} = \theta_{Sk}^{int}$ when the system enters the moving crystal phase. (b) $\sigma_{||}$ (upper blue curve) and $\sigma_\perp$ (lower red curve) vs $F_D$. $\sigma_{||} \approx \sigma_\perp$ when the system enters the moving crystal state, where the velocity fluctuations are isotropic. The labels d, e, and f indicate the values of $F_D$ at which the structure factors in Fig. 5(d,e,f) were obtained. (c) $P_4$ (lower green curve), $P_5$ (central light orange curve), $P_6$ (upper black curve), and $P_7$ (central dark red curve) vs $F_D$ showing a transition to the moving crystal state near $F_D = 2.5$. Inset: $P_6$ vs $F_D$ for systems with $\theta_{Sk}^{int} = 0°$ (gray curve) and $\theta_{Sk}^{int} = 45°$ (black curve) over the range $2.0 < F_D < 4.0$. The $\theta_{Sk}^{int} = 45°$ system reaches a higher saturation value of $P_6 = 0.96$ at $F_D = 2.5$.

FIG. 4. Results from a system with $\theta_{Sk}^{int} = 70°$. (a) $\langle|\mathbf{V}|\rangle$ vs $F_D$. The inset shows $\theta_{Sk}$ vs $F_D$ where $\theta_{Sk} = 0$ at $F_D = 0$ and increases to $\theta_{Sk} = \theta_{Sk}^{int}$ when the system enters the moving crystal phase. (b) $\sigma_{||}$ (upper left blue curve) and $\sigma_\perp$ (lower left red curve) vs $F_D$ showing that the velocity fluctuations become isotropic at high drives. The labels g, h, and i indicate the values of $F_D$ at which the structure factors in Fig. 5(g,h,i) were obtained. Inset: A zoom of the main panel highlighting the small jump in $\sigma_\perp$ at the transition from the moving liquid to the moving crystal. (c) $P_4$ (lower green curve), $P_5$ (central light orange curve), $P_6$ (upper black curve), and $P_7$ (central dark red curve) vs $F_D$ showing a multi-step transition to the moving crystal state near $F_D = 2.75$.

the skyrmions have depinned. The drive dependence of $\theta_{Sk}$ is in agreement with previous simulation studies[51] and experiments[14] which show an increase in $\theta_{Sk}$ with driving force and a saturation to the intrinsic value $\theta_{Sk}^{int}$ at high drives.

The same quantities as above for a system with $\theta_{Sk}^{int} = 70°$ appear in Fig. 4. $\langle|\mathbf{V}|\rangle$ versus $F_D$ in Fig. 4(a) has
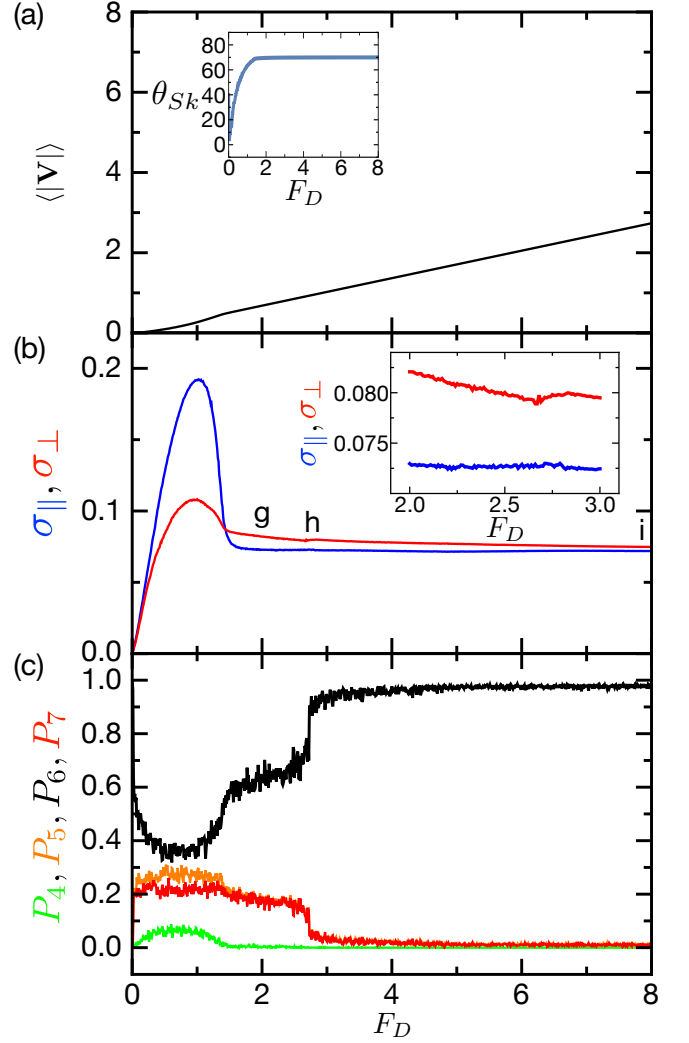
a similar nonlinear shape for $F_D < 2$ as found for the other values of $\theta_{Sk}^{int}$, and at higher drives the magnitude of $\langle|\mathbf{V}|\rangle$ is further decreased compared to the vortex system. The inset of Fig. 4(a) indicates that at low drives $\theta_{Sk} = 0$, while the skyrmion Hall angle saturates to the value $\theta_{Sk} = \theta_{Sk}^{int} = 70°$ at $F_D = 1.5$. In Fig. 4(b), the plot of $\sigma_{||}$ and $\sigma_\perp$ versus $F_D$ shows that there is a sharp decrease in both quantities when the system enters the moving liquid phase at $F_D = 1.5$, and that at high drives $\sigma_\perp$

is slightly larger than $\sigma_{||}$. The plot of $P_4$, $P_5$, $P_6$, and $P_7$ versus $F_D$ in Fig. 4(c) indicates that there are two distinct disordered flowing phases. For $0.3 < F_D < 1.5$, the system exhibits plastic flow (PF) where not all of the skyrmions are moving, $\sigma_{||} > \sigma_{\perp}$, $P_6 = 0.4$, $P_4 > 0$, and $P_5 > P_7$. In contrast, for $1.5 < F_D < 2.5$ the system forms what we call a moving liquid (ML) phase in which all of the skyrmions have depinned and have gained some partial order, with $P_6 \approx 0.625$, $P_4 = 0$, and $P_5 = P_7$ indicating that all the remaining dislocations have formed pairs. For $F_D > 2.5$ the system dynamically orders into a moving crystal as shown by the jump in $P_6$ to $P_6 \approx 0.98$ and the drop in $P_5$ and $P_7$ to $P_5 = P_7 \approx 0.02$. At the transition from the moving liquid to the moving crystal there is also a small jump in $\sigma_{\perp}$, as shown in the inset of Fig. 4(b).

### A. Moving Lattice Structure

The different features in the transport curves and velocity noise fluctuations correlate with changes in the static structure factor $S(\boldsymbol{q})$. In Fig. 5(a,b,c) we plot $S(\boldsymbol{q})$ for the overdamped system with $\theta_{Sk}^{int} = 0°$ from Fig. 2 at drives of $F_D = 1.3$, 2.0, and 8.0, respectively. At $F_D = 1.3$ the system is undergoing plastic flow and $S(\boldsymbol{q})$ in Fig. 5(a) exhibits a ring feature indicative of an amorphous structure, while at $F_D = 2.0$ in Fig. 5(b) the system is in a moving smectic state in which the particles travel in one-dimensional chains that slide past one another, producing two peaks in $S(\boldsymbol{q})$ along the $q_x = 0$ axis. At $F_D = 8.0$ in Fig. 5(c) there is more order in the system as indicated by the additional smeared peaks appearing in $S(\boldsymbol{q})$; however, the system is still in a moving smectic or a strongly anisotropic moving crystal state as shown by the anisotropy in $\sigma_{\perp}$ and $\sigma_{||}$ in Fig. 2(b). This result is in agreement with previous simulations and experiments in the overdamped limit for vortex systems[37–39].

In Fig. 5(d,e,f) we plot $S(\boldsymbol{q})$ for the system in Fig. 3 with $\theta_{Sk}^{int} = 45°$ at drives of $F_D = 1.6$, 2.4 and 8.0. At $F_D = 1.6$ in Fig. 5(d) the system is in a moving liquid phase, while at $F_D = 2.4$ in Fig. 5(e) the system has dynamically ordered into a slightly anisotropic moving crystal phase. Here $S(\boldsymbol{q})$ is rotated compared to the $\theta_{Sk}^{int} = 0°$ case in Fig. 5(b) since the skyrmion lattice is moving at an angle with respect to the drive direction. There is weak anisotropy in the moving structure as indicated by the smearing of four of the peaks in $S(\boldsymbol{q})$, which is consistent with the small anisotropy observed in $\sigma_{\perp}$ and $\sigma_{||}$ for this drive value in Fig. 3(b). At $F_D = 8.0$ in Fig. 5(f) where $\sigma_{\perp} = \sigma_{||}$, the system forms a moving crystal state in which all six peaks in $S(\boldsymbol{q})$ have almost equal weight. In Fig. 5(g,h,i) we plot $S(\boldsymbol{q})$ for the system in Fig. 4 with $\theta_{Sk}^{int} = 70°$ at drives of $F_D = 2.0$, 2.8, and 8.0, respectively. Similar to the $\theta_{Sk}^{int} = 45°$ case, at $F_D = 2.0$ in Fig. 5(g) the system forms a disordered moving liquid state, at $F_D = 2.8$ in Fig. 5(h) a slightly anisotropic moving crystal state appears, and at

high drives of $F_D = 8.0$ in Fig. 5(i), an isotropic moving crystal forms as indicated by the equal weight of the six peaks in $S(\boldsymbol{q})$.

In Fig. 6 we plot a dynamic phase diagram as a function of $\theta_{Sk}^{int}$ versus $F_D$. For $F_D/F_p < 1.0$ there is a mixture of pinned and moving skyrmions and we find a plastic flow (PF) phase with a disordered structure. In this regime, the velocity fluctuations are anisotropic with $\sigma_{||} > \sigma_{\perp}$, and $\theta_{Sk}$ increases from zero as $F_D$ increases. Just above $F_D/F_p = 1.0$, all the skyrmions are moving but the structure is still disordered, placing the system in a moving liquid (ML) phase. The value of $\theta_{Sk}$ saturates to $\theta_{Sk} = \theta_{Sk}^{int}$ at the onset of the ML phase. For $\theta_{Sk}^{int} < 10°$, at higher drives the system transitions into the same moving smectic (MS) state found in the vortex system. At $\theta_{Sk}^{int} = 10°$ we find that the ML-MS transition is followed at slightly higher $F_D$ by a transition into a moving crystal (MC) phase. In the MC phase the fluctuations are isotropic or only slightly anisotropic with $\sigma_{\perp} \gtrsim \sigma_{||}$. For $10° < \theta_{Sk}^{int} \leq 70°$ we find no MS phase and the system transitions directly from the ML phase to the MC phase. For $\theta_{Sk}^{int} = 80°$, above the PF-ML transition the system remains in the ML phase out to the highest values of $F_D$ we have considered; however, in principle it is possible that the system could dynamically order at much higher drives. At $\theta = 0°$, the ML phase extends from $F_D = 1.5$, when all the particles depin, to $F_D = 1.8$. Both $P_5$ and $P_7$ decrease throughout the ML regime before reaching a partial saturation at the onset of the MS phase, as shown in Fig. 2.

The loss of the MC phase at large values of $\theta_{Sk}^{int}$ is due to the nondissipative nature of the Magnus term which becomes increasingly dominant as the intrinsic skyrmion Hall angle increases, creating larger dynamical fluctuations that prevent the skyrmions from reordering due to what we term a Magnus melting effect.

### B. Diffusion

For vortex systems, the dynamic fluctuations of the vortices induced by interactions with the pinning sites are argued to act as an anisotropic effective shaking temperature, with the largest fluctuations occurring along the driving direction. In order to test the nature of the fluctuations we measure the mean squared displacement (MSD) of the skyrmions by projecting the individual skyrmion displacements into the directions parallel and perpendicular to the drive-dependent $\theta_{Sk}$ direction. We define the parallel MSD in the center-of-mass frame of reference at time $t$ as $\Delta_{||}(t) = N^{-1} \sum_{i=1}^{N} \left[ \tilde{r}_{i,||}(t) - \tilde{r}_{i,||}(0) \right]^2$, where $\tilde{r}_{i,||}(t) = r_{i,||}(t) - R_{||}^{CM}(t)$. Similarly, the perpendicular MSD in the center-of-mass frame of reference is given by $\Delta_{\perp}(t) = N^{-1} \sum_{i=1}^{N} \left[ \tilde{r}_{i,\perp}(t) - \tilde{r}_{i,\perp}(0) \right]^2$, where $\tilde{r}_{i,\perp}(t) = r_{i,\perp}(t) - R_{\perp}^{CM}(t)$. Here we have used the parallel and perpendicular components of the position of the $i$-th skyrmion
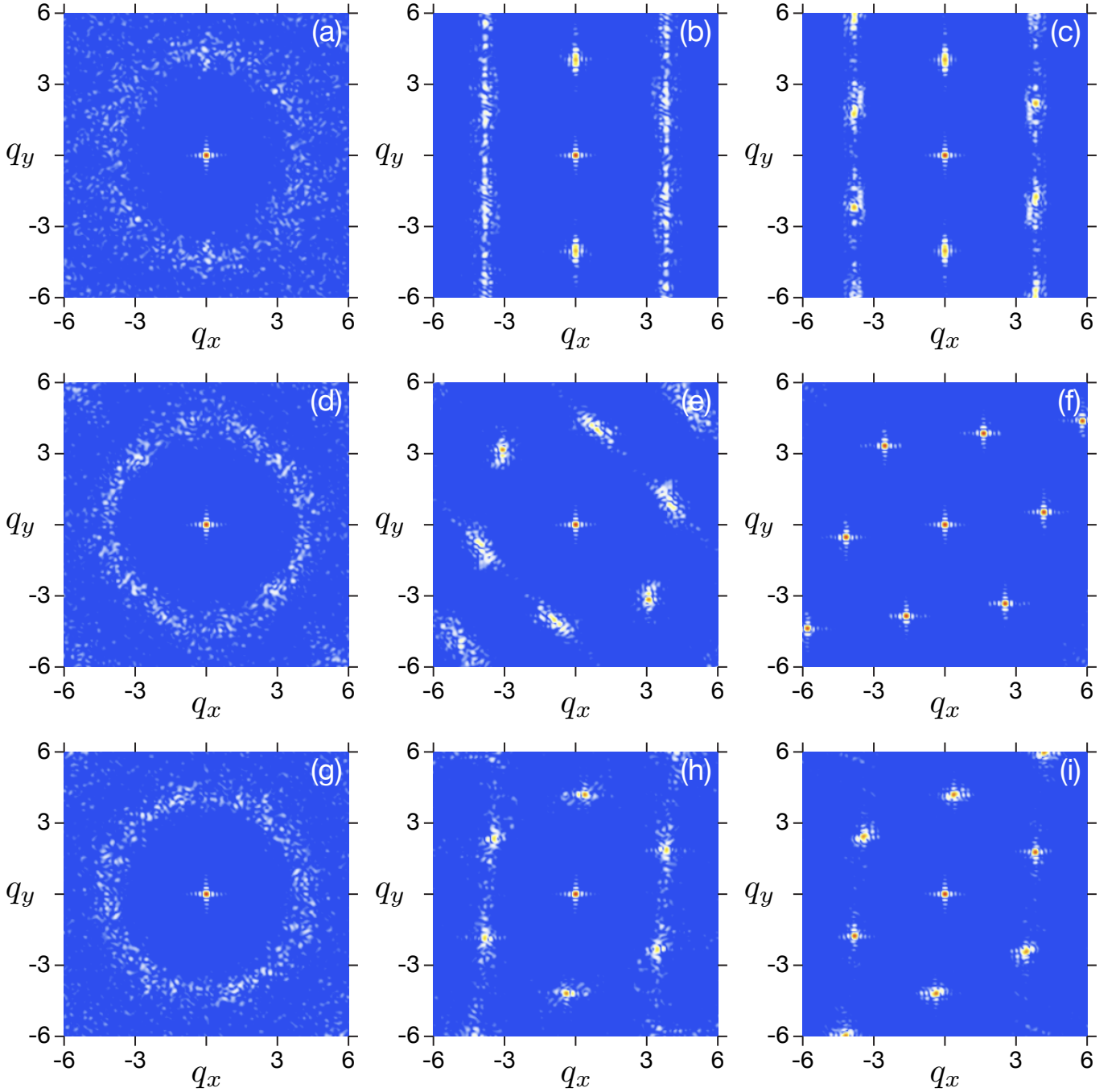
FIG. 5. Static structure factors $S(\boldsymbol{q})$. (a,b,c) The system in Fig. 2 with $\theta_{Sk} = 0°$ at drives of (a) $F_D = 1.3$ in the plastic flow state, (b) $F_D = 2.0$ in the moving smectic state, and (c) $F_D = 8.0$ in the moving anisotropic crystal state. (d,e,f) The system in Fig. 3 with $\theta_{Sk} = 45°$ at drives of (d) $F_D = 1.6$ in the moving liquid state, (e) $F_D = 2.4$ in a slightly anisotropic moving crystal state, and (f) $F_D = 8.0$ in the moving crystal state. (g,h,i) The system in Fig. 4 with $\theta_{Sk} = 70°$ at drives of (g) $F_D = 2.0$ in the moving liquid state, (h) $F_D = 2.8$ in a slightly anisotropic moving crystal state, and (i) $F_D = 8.0$ in the moving crystal state.

and of the center of mass $\boldsymbol{R}^{\mathrm{CM}}$. These components are given by $r_{i,\|} = \boldsymbol{r}_i \cdot \hat{\boldsymbol{x}} \cos\theta_{Sk} + \boldsymbol{r}_i \cdot \hat{\boldsymbol{y}} \sin\theta_{Sk}$, $r_{i,\perp} = \boldsymbol{r}_i \cdot \hat{\boldsymbol{y}} \cos\theta_{Sk} - \boldsymbol{r}_i \cdot \hat{\boldsymbol{x}} \sin\theta_{Sk}$, and similarly for $\boldsymbol{R}^{\mathrm{CM}}$. The position of the center of mass is $\boldsymbol{R}^{\mathrm{CM}} = N^{-1} \sum_{i=1}^{N} \boldsymbol{r}_i$.

At long times, $\Delta_\|(t)$ and $\Delta_\perp(t)$ exhibit a power law

behavior and are proportional to $t^\alpha$, where $\alpha$ is the diffusion exponent. We write $\Delta_\|(t) \propto t^{\alpha_\|}$ and $\Delta_\perp(t) \propto t^{\alpha_\perp}$.

In Fig. 7(a) we plot $\Delta_\|$ and $\Delta_\perp$ versus time for the overdamped case of $\theta_{Sk}^{int} = 0°$ at a drive of $F_D = 4.0$ where the system forms a moving smectic state. Here
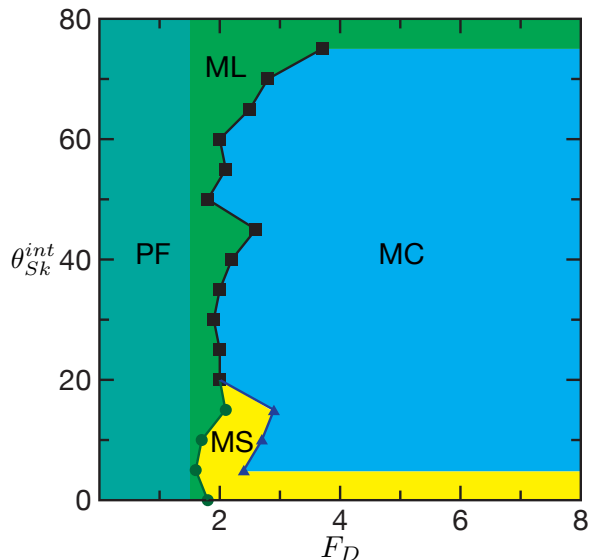
FIG. 6. Dynamic phase diagram as a function of the intrinsic skyrmion Hall angle $\theta_{Sk}^{int}$ vs the drive strength $F_D$. PF: plastic flow phase; ML: moving liquid phase; MS: moving smectic phase; and MC: moving crystal phase. The line separating PF from ML is at $F_D = F_p$. For $F_D < F_p$, only a portion of the skyrmions are flowing, while for $F_D \geq F_p$, all of the skyrmions are moving. At high $\theta_{Sk}^{int}$ the MC phase is lost due to a Magnus melting effect. Black squares indicate the ML-MC boundary, green circles mark the ML-MS boundary, and blue triangles show the location of the MS-MC boundary.

$\Delta_{||} \gg \Delta_{\perp}$ and power law fits of the long time behavior give $\alpha_{||} \approx 2$, consistent with ballistic motion in the parallel direction, and $\alpha_{\perp} = 0.04$. This result is in agreement with previous simulation studies measuring the diffusive behavior in the moving smectic phase for vortices in type-II superconductors[40]. The superdiffusive behavior of $\Delta_{||}$ arises due to the fact that in the moving smectic state the particles move in one-dimensional chains that slip past each other due to their slightly different velocities. As a result, the distance between any two particles in different chains in the moving center of mass frame grows linearly with time. Since there is no transverse hopping of particles from chain to chain, diffusion perpendicular to the driving direction is strongly suppressed. In Fig. 7(b) we plot $M_{||}$ and $M_{\perp}$, the value of $\Delta_{||}$ and $\Delta_{\perp}$ at a time of $\tau = 5 \times 10^5$ simulation time steps, versus $F_D$ for the $\theta_{Sk}^{int} = 0°$ system in Fig. 7(a). Here $M_{||} > M_{\perp}$ for all $F_D$, and there is a drop in $M_{\perp}$ at the ML-MS transition. Within the ML phase, $\Delta_{\perp}$ behaves diffusively while in the MS phase it has subdiffusive behavior (not shown).

In Fig. 7(c) we plot $\Delta_{||}$ and $\Delta_{\perp}$ versus time for a system with $\theta_{Sk}^{int} = 45°$ at $F_D = 4.0$ in the moving crystal phase. Here the displacements are isotropic and we find subdiffusive behavior with $\alpha_{||} \approx \alpha_{\perp} \approx 0.45$. In general, in the moving crystal phase a small number of dislocations are present that can slowly climb or glide, producing the weak subdiffusive behavior in both $\Delta_{||}$ and $\Delta_{\perp}$.

The plot of $M_{||}$ and $M_{\perp}$ versus $F_D$ in Fig. 7(d) indicates that the displacements are anisotropic in the PF phase for $F_D < 2.0$, and then become isotropic in the MC phase for $F_D \geq 2.0$. These results indicate that the isotropic nature of the effective shaking temperature in the moving skyrmion system is responsible for the formation of an isotropic moving crystal phase. Figure 7(e) shows $\Delta_{||}$ and $\Delta_{\perp}$ versus time in the moving crystal phase at $F_D = 4.0$ for a system with $\theta_{Sk}^{int} = 70°$. We find subdiffusive behavior in both directions with $\alpha_{||} \approx \alpha_{\perp} \approx 0.22$, and $\Delta_{\perp}$ is slightly larger than $\Delta_{||}$. In Fig. 7(f) we show $M_{||}$ and $M_{\perp}$ versus $F_D$ for the same system, where we observe a transition to isotropic diffusion at the higher drives. At $\theta_{Sk}^{int} = 80°$ where the moving liquid phase persists up to high drives, there is still a transition from anisotropic diffusion in the plastic flow phase to isotropic diffusion in the ML phase; however, within the ML phase $\alpha_{||}$ and $\alpha_{\perp}$ have much higher values than what we observe in the MC phase for smaller $\theta_{Sk}^{int}$. This indicates that even within the disordered flow regime, the Magnus dominated dynamics modify the diffusive behavior compared to what is observed in the overdamped case.

## C. Small Intrinsic Skyrmion Hall Angles

The small intrinsic skyrmion Hall angle case of $\theta_{Sk}^{int} = 10°$ is particularly interesting since it exhibits both a MS and a MC phase. In Fig. 8(a) we plot $\Delta_{\perp}$ and $\Delta_{||}$ as a function of time for the $\theta_{Sk}^{int} = 10°$ system at $F_D = 2.0$ in the MS phase. Here $\Delta_{||}$ is superdiffusive with $\alpha_{||} = 1.54$ while $\Delta_{\perp}$ is subdiffusive with $\alpha_{\perp} = 0.24$. Figure 8(b) shows that the structure factor at $F_D = 2.0$ contains prominent peaks indicative of a smectic ordering. The moving smectic is tilted with respect to the $x$ axis since the skyrmions are moving at an angle $\theta_{Sk} \approx 9.8°$ relative to the driving direction. This differs from the MS that forms for $\theta_{Sk}^{int} = 0°$, shown in Fig. 5(b), which remains aligned with the drive direction. In Fig. 8(c), a Voronoi construction of the instantaneous skyrmion positions in the MS phase indicates that the defects assemble into 5-7 pairs that glide along the direction in which the skyrmions are moving.

At $F_D = 2.75$, a transition occurs into the MC state where the skyrmions move at an angle $\theta_{Sk} = 10°$ to the driving direction, indicating that the MS-MC transition is also associated with a lattice rotation. In Fig. 8(d) the plot of $\Delta_{\perp}$ and $\Delta_{||}$ versus time in simulation steps at $F_D = 4.0$ in the MC state shows that the system is much more isotropic and that both $\Delta_{\perp}$ and $\Delta_{||}$ exhibit subdiffusive behavior with $\alpha_{||} \approx \alpha_{\perp} \approx 0.425$. The corresponding structure factor in Fig. 8(e) contains six peaks with equal weight. In general the moving crystal phases are considerably more ordered than the moving smectic phase, as illustrated by the Voronoi construction of the instantaneous skyrmion positions in the MC phase shown in Fig. 8(f), where there are significantly fewer 5-7 dislocation pairs compared to the MS phase. Additionally, the
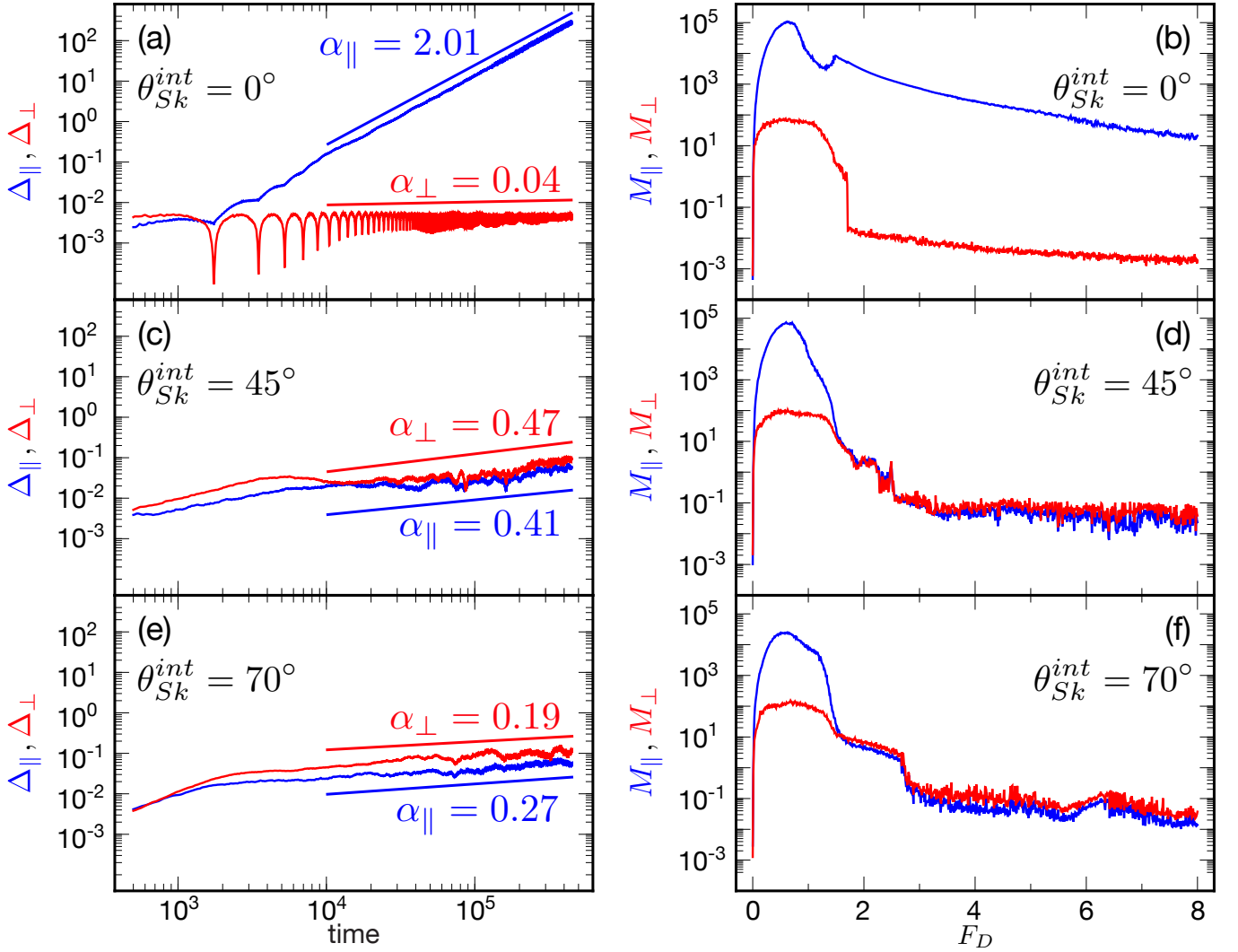
FIG. 7. (a,c,e) The parallel and perpendicular mean square displacements, $\Delta_{||}$ (blue) and $\Delta_\perp$ (red), vs time in simulation steps obtained at $F_D = 4.0$. (a) At $\theta_{Sk}^{int} = 0°$ in the moving smectic phase, the diffusion exponents are $\alpha_{||} = 2.01$ and $\alpha_\perp = 0.04$. (c) At $\theta_{Sk}^{int} = 45°$ in the moving crystal phase, $\alpha_{||} = 0.41$ and $\alpha_\perp = 0.47$. (e) At $\theta_{Sk}^{int} = 70°$ in the moving crystal phase, $\alpha_{||} = 0.27$ and $\alpha_\perp = 0.19$. (b,d,f) $M_{||} = \Delta_{||}(\tau)$ and $M_\perp = \Delta_\perp(\tau)$ vs $F_D$ with $\tau = 5 \times 10^5$ simulation time steps. (b) $\theta_{Sk}^{int} = 0°$, (d) $\theta_{Sk}^{int} = 45°$, and (f) $\theta_{Sk}^{int} = 70°$. As the intrinsic skyrmion Hall angle increases, the Magnus term becomes dominant over the dissipation and the anisotropy in $\Delta_{||}$ and $\Delta_\perp$, which serve as measures of the effective temperatures parallel and perpendicular to $\theta_{Sk}$, is greatly reduced.

dislocations in the MC are not aligned with the direction of motion and can move slowly in any of the six symmetry directions of the skyrmion lattice, leading to the subdiffusive behavior. It is possible that for even smaller but finite values of $\theta_{Sk}^{int}$, MS-MC transitions could occur that are pushed to higher values of $F_D$ as $\theta_{Sk}^{int}$ decreases. Although skyrmion systems generally have $\theta_{Sk}^{int} > 25°$, a finite but small Magnus term can still arise in some vortex systems, so it may be possible to observe MS-MC transitions in superconducting systems, particularly for weak pinning where large vortex velocities could be realized.

## IV. NOISE SIGNATURES

We next analyze the velocity noise power spectral densities, $S_{||}(\omega)$ and $S_\perp(\omega)$, computed from time series taken at fixed $F_D$ of the velocity fluctuations parallel and perpendicular to $\theta_{Sk}$, respectively. In Fig. 9(a,b,c) we plot $S_{||}(\omega)$ and $S_\perp(\omega)$ for the overdamped case of $\theta_{Sk}^{int} = 0°$ at $F_D = 1.0$ in the plastic flow regime, $F_D = 2.0$ in the moving smectic phase, and at $F_D = 4.0$ in the moving smectic phase. At $F_D = 1.0$, we find broad band noise in both directions with the largest noise power in the parallel direction. $S_{||}(\omega)$ has a $1/\omega$ feature at low frequencies along with a $1/\omega^2$ tail at high frequencies, while $S_\perp(\omega)$
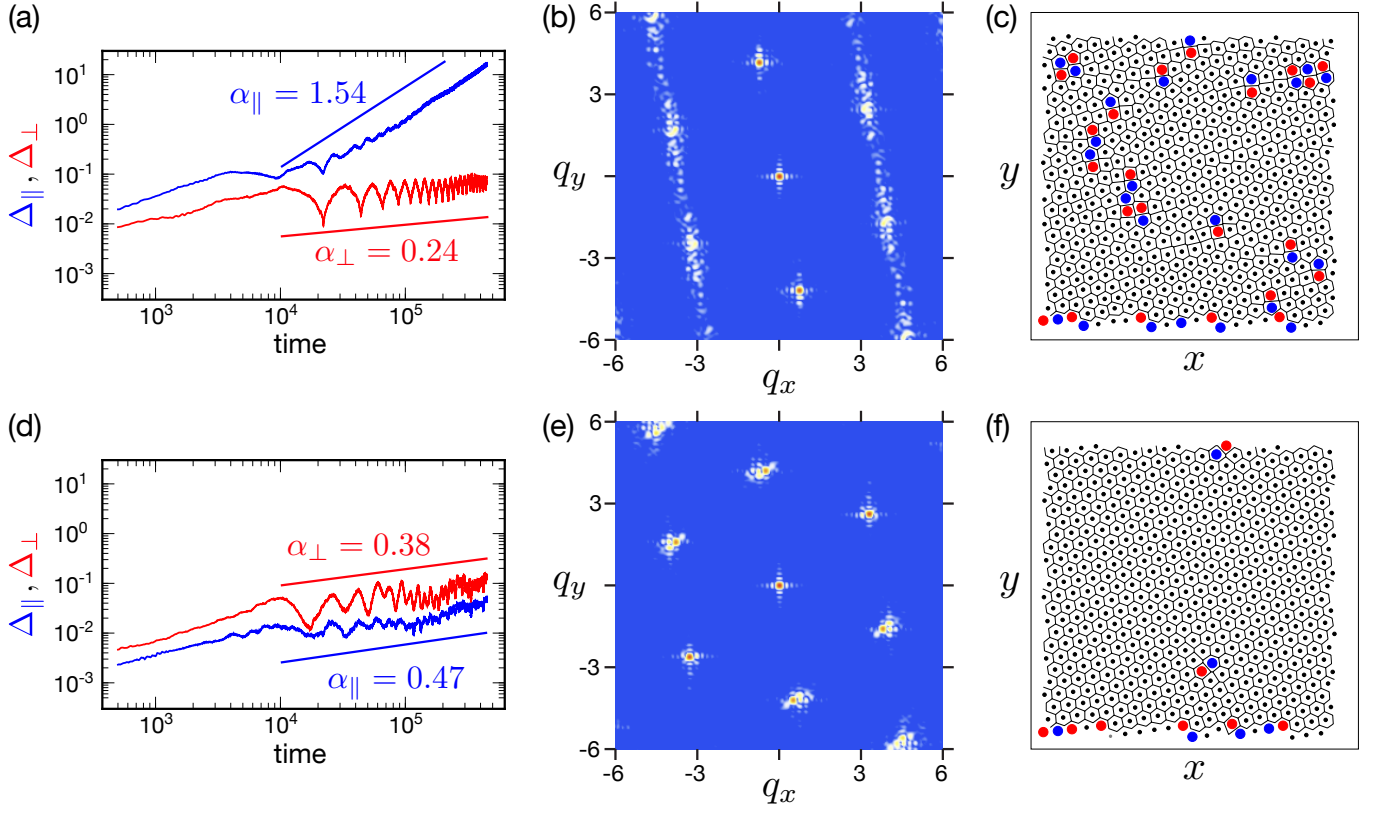
FIG. 8. The transition from a moving smectic to a moving crystal for a system with $\theta_{Sk}^{int} = 10°$. (a) $\Delta_{||}$ (upper blue line) and $\Delta_{\perp}$ (lower red line) vs time in simulation time steps at $F_D = 2.0$ in the moving smectic phase. $\alpha_{||} = 1.54$, indicating superdiffusive behavior, while $\alpha_{\perp} = 0.24$, indicating subdiffusive behavior. (b) The corresponding structure factor $S(\boldsymbol{q})$. (c) Voronoi construction of the instantaneous skyrmion positions at $F_D = 2.0$. Black dots indicate sixfold-coordinated skyrmions, red dots indicate fivefold-coordinated skyrmions, and blue dots indicate sevenfold-coordinated skyrmions. In the smectic state, the defects combine into 5-7 pairs that glide along the driving direction. (d) $\Delta_{||}$ (lower blue line) and $\Delta_{\perp}$ (upper red line) vs time in simulation time steps at $F_D = 4.0$ in the moving crystal phase. (e) The corresponding structure factor $S(\boldsymbol{q})$. (f) The corresponding Voronoi construction of the instantaneous skyrmion positions at $F_D = 4.0$ shows an almost completely ordered lattice.

becomes white at low frequencies. At $F_D = 2.0$ in the moving smectic state, characteristic frequencies emerge which become more pronounced at $F_D = 4.0$. We find a washboard frequency of $\omega \approx 14.5$ at $F_D = 4.0$ that is produced by the perturbations of the periodic vortex lattice by the underlying pinning sites. This frequency corresponds to $\omega = 2\pi\langle|\mathbf{V}|\rangle/a$, where $a$ is the characteristic spacing between the vortices in the driving direction. We also observe a time-of-flight signal at $\omega = 2\pi\langle|\mathbf{V}|\rangle/L_x$ which produces weaker peaks with $\omega < 1$. In superconducting systems both of these frequencies have been measured in experiments and simulations. In Fig. 9(d,e,f) we plot $S_{||}(\omega)$ and $S_{\perp}(\omega)$ for a system with $\theta_{Sk}^{int} = 45°$ at $F_D = 1.0$, 2.0, and 4.0, respectively. At $F_D = 1.0$ in the plastic flow regime we again find a broad band noise signal, but the anisotropy between $S_{||}(\omega)$ and $S_{\perp}(\omega)$ is smaller than in the overdamped case. In the moving crystal phase, at $F_D = 2.0$ the noise is isotropic and a narrow band frequency emerges which becomes sharper at $F_D = 4.0$. In Fig. 9(g,h,i) we show $S_{||}(\omega)$ and $S_{\perp}(\omega)$ for a system with $\theta_{Sk}^{int} = 70°$ at $F_D = 1.0$, 2.0, and 4.0, respec-

tively. At $F_D = 2.0$ the system is in a ML phase and the noise power is flat at low frequencies, while at $F_D = 4.0$ we find a strong washboard signal in both directions with slightly higher signal strength at higher frequencies in the perpendicular direction. These results indicate that moving skyrmion lattices can exhibit a narrow band noise signature similar to that found in the vortex system, and that analysis of this noise could be used to extract the lattice constant and skyrmion velocity.

Another feature produced in the noise signatures by a finite Magnus term is switching events that are associated with global rotations in the moving skyrmion structures. These switching events occur due to the drive dependence of the flow direction generated by the Magnus term. Such switching events do not occur in an overdamped system since the lattice remains locked to the driving direction once it has entered the MS phase. In Fig. 10(a) we plot a heightfield showing the magnitude of the $S_{||}$ noise component as a function of $F_D$ versus $\omega$ in the overdamped case of $\theta_{Sk}^{int} = 0°$. The plastic flow regime for $F_D < 1.75$ is distinguished by large ampli-
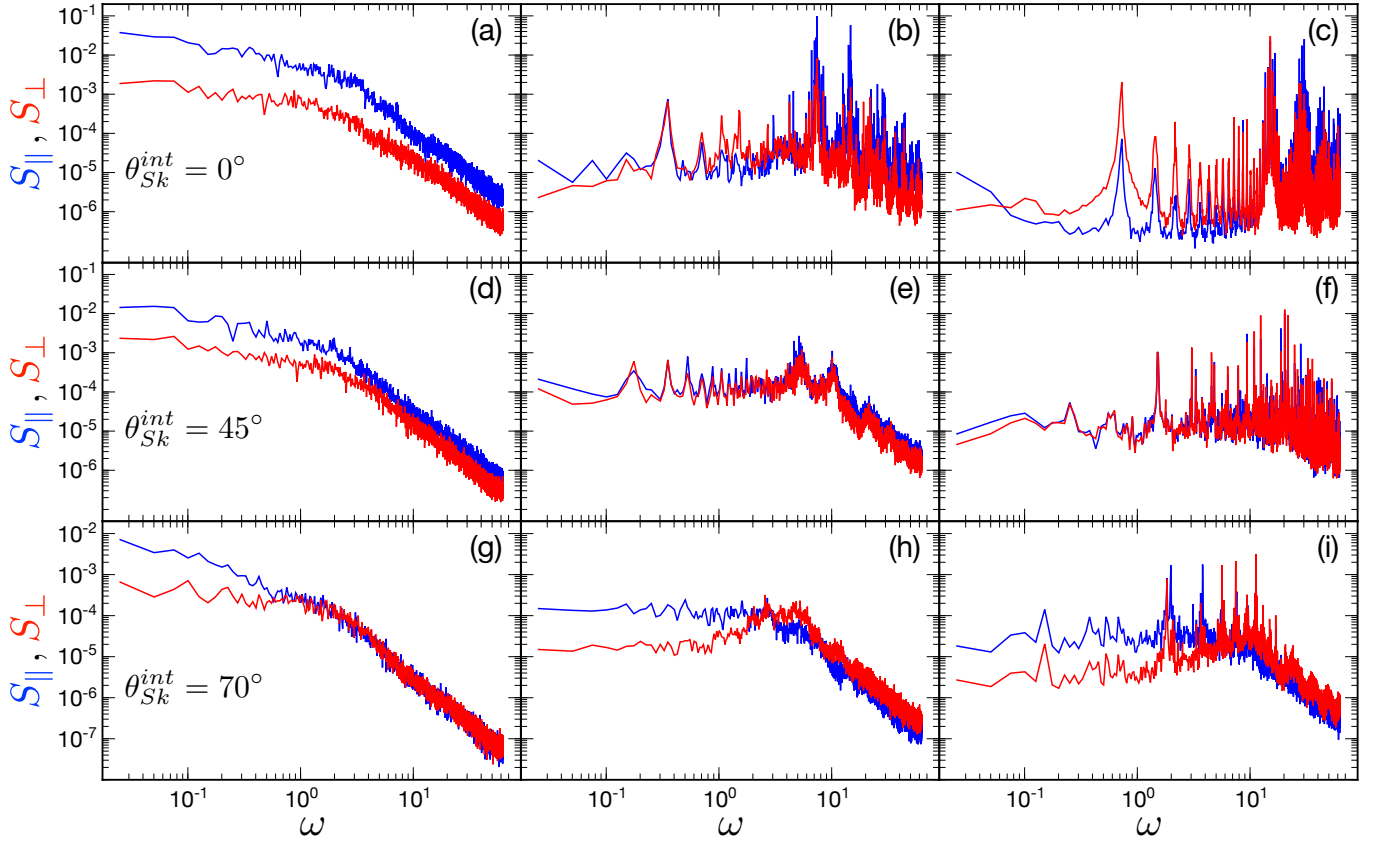
FIG. 9.   Noise power spectral density plots $S_{||}(\omega)$ (blue) for velocity fluctuations parallel to $\theta_{Sk}$ and $S_{\perp}(\omega)$ (red) for velocity fluctuations perpendicular to $\theta_{Sk}$. (a,b,c) A sample with $\theta_{Sk}^{int} = 0°$ at (a) $F_D = 1.0$ in the disordered flow state, (b) $F_D = 2.0$ in the moving smectic phase, and (c) $F_D = 4.0$ in moving smectic phase. (d,e,f) A sample with $\theta_{Sk}^{int} = 45°$ at (d) $F_D = 1.0$ in the disordered flow state, (e) $F_D = 2.0$ in the moving crystal phase, and (f) $F_D = 4.0$ in moving crystal phase. (g,h,i) A sample with $\theta_{Sk}^{int} = 70°$ at (g) $F_D = 1.0$ in the disordered flow state, (h) $F_D = 2.0$ in the moving liquid phase, and (i) $F_D = 4.0$ in the moving crystal phase.

tude low frequency noise, while the onset of the narrow band noise at $F_D = 1.75$ is indicated by a series of lines that shift to higher frequencies with increasing $F_D$. For $\theta_{Sk}^{int} = 45°$, the heightfield plot of $S_{||}$ in Fig. 10(b) shows several switching events that occur near $F_D = 2.25$ as indicated by the horizontal features. Figure 10(c) shows a heightfield plot of $S_{||}$ for $\theta_{Sk}^{int} = 70°$. Here the plastic phase appears as a strong signal at low frequency for $F_D < 1.5$, while for $1.5 < F_D < 2.8$ the system is in the moving liquid phase. The dashed line at $F_D = 2.85$ denotes the transition into the MC phase, while the dashed line at $F_D = 4.85$ indicates a switching event. We measure $\phi_n$, the angle between the $n$th structure factor peak and the $x$ axis, for the $\theta_{Sk}^{int} = 70°$ system, and plot $\phi_1$, $\phi_2$, and $\phi_3$ for the peaks in the first two quadrants versus $F_D$ in Fig. 10(g). The two dashed lines are at the same values of $F_D$ as the dashed lines in Fig. 10(c). The first dashed line at $F_D = 2.85$ indicates that just after the moving crystal forms, there is a switching event in the lattice orientation, while the dashed line at $F_D = 4.85$ shows that there is a second switching event associated with a lattice rotation. In Fig. 10(c), several of the narrow band

noise peaks disappear above the second switching event.

Figure 10(d) shows a heightfield plot of $S_{||}(\omega)$ versus $F_D$ at $\theta_{Sk}^{int} = 10°$ where a frequency shift is associated with the MS-MC transition. The region in which the MS phase appears is bounded by the two dashed lines. Once the system enters the MC phase, several additional narrow band noise peaks arise. The plot of $\theta_{Sk}$ versus $F_D$ for the $\theta_{Sk}^{int} = 10°$ system in Fig. 10(e) shows that there is a jump in $\theta_{Sk}$ to $\theta_{Sk} = 9.8°$ at the transition to the MC phase. We measure the magnitude $h_n$ of individual peaks in the structure factor $S(\mathbf{q})$ and plot $h_1$, $h_2$, and $h_3$ versus $F_D$ for the three peaks in the first and second quadrants in Fig. 10(f) for the same system. In the MS phase, only $h_2$ is large, indicating the strong asymmetry of the weight of the peaks due to the smectic ordering. At the transition to the MC phase, all the peaks in the structure factor have similar weights. These results indicate that switching events in the noise spectral power measurements can be used to deduce information about the lattice orientation.
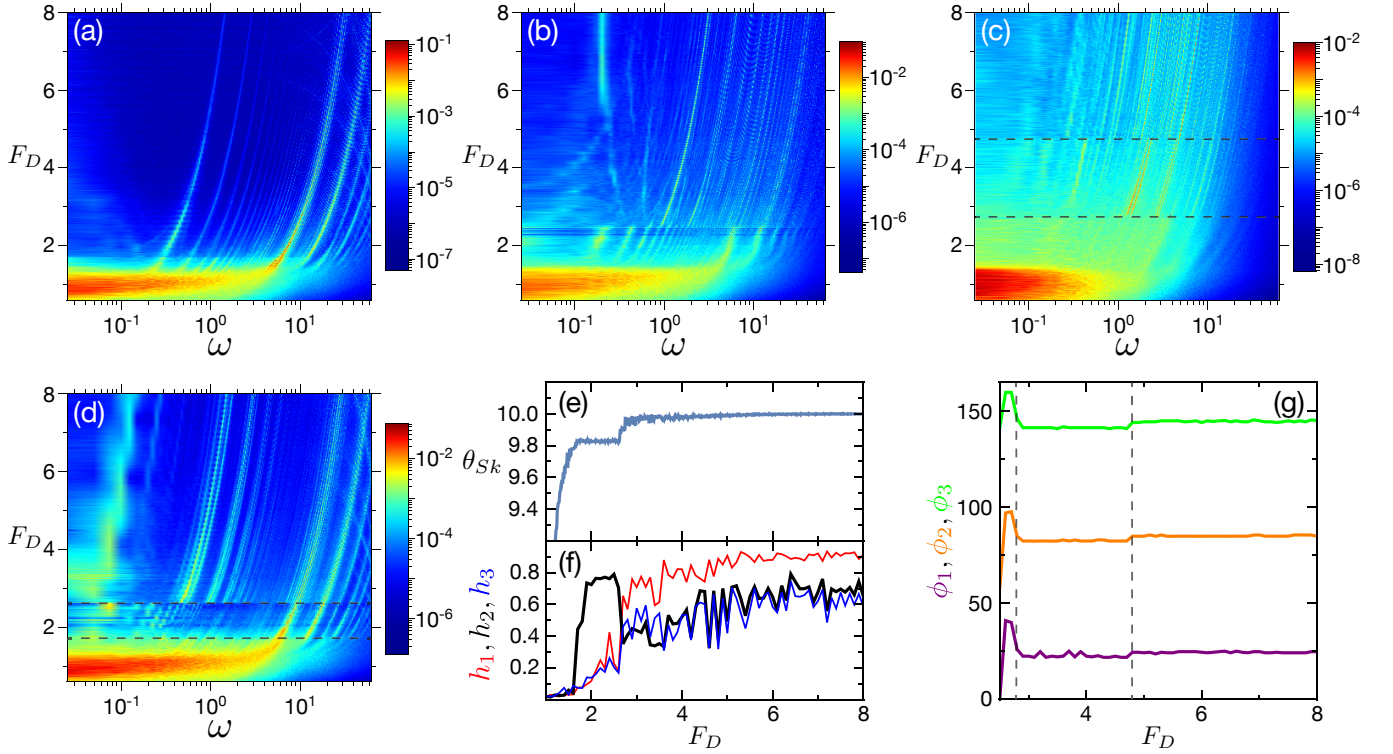
FIG. 10. (a,b,c,d) Heightfield plots of the power spectral density $S_{||}$ as a function of $F_D$ and $\omega$. (a) $\theta_{Sk}^{int} = 0°$. (b) $\theta_{Sk}^{int} = 45°$. (c) $\theta_{Sk}^{int} = 70°$, where the two dashed lines indicate the switching events illustrated in panel (g). (d) $\theta_{Sk}^{int} = 10°$, where there is a MS phase in the region between the two dashed lines. (e) $\theta_{Sk}$ vs $F_D$ at $\theta_{Sk}^{int} = 10°$. (f) The structure factor peak heights $h_1$ (red), $h_2$ (black), and $h_3$ (blue) vs $F_D$ in a system with $\theta_{Sk}^{int} = 10°$. Pairs of peaks $180°$ apart are indistinguishable in the plotted range, shown are those corresponding to the first two quadrants. At large drives, peak $h_1$ is at an angle $\phi_1 = 40°$ with respect to the $x$ axis, peak $h_2$ is at $\phi_2 = 100°$, and peak $h_3$ is at $\phi_3 = 160°$. (g) The angles $\phi_1$, $\phi_2$, and $\phi_3$ at which three of the structure factor peaks appear vs $F_D$ for the system in panel (c) with $\theta_{Sk}^{int} = 70°$. The two dashed lines indicate switching events that are associated with a lattice rotation.

## V. DISCUSSION

We have only considered the case of rigid skyrmions; however, it is possible that internal modes or distortions could arise that would modify the transport signatures. In Ref.[15] it is argued that distortions in the skyrmion shape as a function of current or drive can change the skyrmion Hall effect. For example, if the skyrmions become elongated, the fluctuations would be more anisotropic and this could make the skyrmion-skyrmion interactions anisotropic, which would tend to stabilize moving smectic phases rather than moving crystal phases at higher drives. Since narrow band noise appears in both the moving smectic and moving crystal phases, velocity noise measurements are a robust probe of changes in the ordering of the moving skyrmions. Additionally, the switching events in the noise spectral power should be a robust feature. It is also possible for breathing modes to appear in the moving skyrmion state which are not included in the particle-based model. These could introduce additional dynamical modes which could couple to the velocity noise modes; alternatively, the breathing mode frequencies could be much higher than those of

the velocity noise and would appear as additional noise peaks.

Future studies could examine such skyrmion dynamics using continuum models, which are computationally expensive and more difficult to use for probing low frequency effects. Another approach would be to add correlated fluctuations mimicking the dynamical effects to the continuum models in order to reduce the computational resource requirements.

Although the diffusive behavior we observe is generated dynamically, we can compare our results to equilibrium thermal studies of skyrmions[57,58], which show that the Magnus force reduces the diffusion since the particles move in more circular patterns rather than diffusing outward as in the overdamped case. In our system, under high drives the fluctuations experienced by the skyrmions produce a reduced diffusion, leading to the appearance of a moving crystal, whereas in an overdamped system, there is still strong diffusion along the direction of drive, causing a moving smectic state to form.

## VI. SUMMARY

We have numerically examined the velocity fluctuations parallel and perpendicular to the direction of motion for skyrmions driven over random disorder for different values of the Magnus term or intrinsic skyrmion Hall angle. In the overdamped limit, the system undergoes a transition from a disordered phase to a moving smectic state in which the velocity fluctuations are strongly anisotropic and have the largest magnitude parallel to the direction of motion. In the center of mass frame of the smectic state, the particle displacements are either diffusive or superdiffusive in the direction of motion but subdiffusive in the perpendicular direction. For a finite intrinsic skyrmion Hall angle, the system is disordered at low drives, while at higher drives it transitions into a moving crystal state which exhibits isotropic velocity fluctuations and has subdiffusive particle displacements in the center of mass frame both parallel and perpendicular to the direction of motion. The isotropic nature of the moving skyrmion crystal is a result of the Magnus term, which generates velocity fluctuations perpendicular to the force fluctuations experienced by the moving skyrmions due to the pinning sites. In general, moving skyrmion lattices are more ordered than moving vortex lattices and the dynamic shaking temperature is isotropic for skyrmions but anisotropic in vortex systems. We show that the velocity noise power spectra can be used to identify the transition from the plastic flow or moving liquid state to the moving crystal state in skyrmion systems since it changes from a broad band noise signal to a narrow band noise signal. In the moving crystal state, velocity noise power peaks appear at the washboard frequency, which permits the calculation of the velocity and lattice spacing of the moving skyrmion lattice. We find that the moving skyrmion lattice can exhibit discrete switching events associated with global lattice reorientations due to the dependence of the skyrmion Hall angle on the magnitude of the external drive. These switching events produce changes in the noise fluctuations as well as rotations in the structure factor. For small but finite intrinsic skyrmion Hall angles, the system exhibits a mixture of both vortex-like and skyrmion-like dynamical behavior. At lower drives the system first dynamically orders into a moving smectic state, but at higher drives there is a transition into a moving crystal which is associated with both a change in the direction of skyrmion motion as well as pronounced changes in the velocity noise signal. Skyrmion velocity fluctuations could be measured by direct imaging of moving skyrmions, measuring fluctuations in the topological Hall resistance, performing magnetic noise measurements with Hall probes, or measuring the time dependence of the structure factor.

[1] S. Mühlbauer, B. Binz, F. Jonietz, C. Pfleiderer, A. Rosch, A. Neubauer, R. Georgii, and P. Böni, Skyrmion lattice in a chiral magnet, Science **323**, 915 (2009).

[2] X.Z. Yu, Y. Onose, N. Kanazawa, J.H. Park, J.H. Han, Y. Matsui, N. Nagaosa, and Y. Tokura, Real-space observation of a two-dimensional skyrmion crystal, Nature (London) **465**, 901 (2010).

[3] N. Nagaosa and Y. Tokura, Topological properties and dynamics of magnetic skyrmions, Nature Nanotechnol. **8**, 899 (2013).

[4] W. Jiang, P. Upadhyaya, W. Zhang, G. Yu, M.B. Jungfleisch, F.Y. Fradin, J.E. Pearson, Y. Tserkovnyak, K.L. Wang, O. Heinonen, S.G.E. te Velthuis, and A. Hoffmann, Blowing magnetic skyrmion bubbles, Science **349**, 283 (2015).

[5] Y. Tokunaga, X.Z. Yu, J.S. White, H.M. Rønnow, D. Morikawa, Y. Taguchi, and Y. Tokura, A. new class of chiral materials hosting magnetic skyrmions beyond room temperature, Nature Commun. **6**, 7638 (2015).

[6] S. Woo, K. Litzius, B. Kruger, M.Y. Im, L. Caretta, K. Richter, M. Mann, A. Krone, R.M. Reeve, M. Weigand, P. Agrawal, I. Lemesh, M.A. Mawass, P. Fischer, M. Klaui, and G.R.S.D. Beach, Observation of room temperature magnetic skyrmions and their current-driven dynamics in ultrathin Co films, Nature Mater. **15**, 501 (2016).

[7] O. Boulle, J. Vogel, H. Yang, S. Pizzini, D. de Souza Chaves, A. Locatelli, T.O. Mentes, A. Sala, L.D. Buda-Prejbeanu, O. Klein, M. Belmeguenai, Y. Roussigné, A. Stashkevich, S.M. Chérif, L. Aballe, M. Foerster, M. Chshiev, S. Auffret, I.M. Miron, and G. Gaudin, Room-temperature chiral magnetic skyrmions in ultrathin magnetic nanostructures. Nature Nanotech. **11**, 449 (2016).

[8] F. Jonietz, S. Mühlbauer, C. Pfleiderer, A. Neubauer, W. Münzer, A. Bauer, T. Adams, R. Georgii, P. Böni, R.A. Duine, K. Everschor, M. Garst, and A. Rosch, Science **330**, 1648 (2010).

[9] T. Schulz, R. Ritz, A. Bauer, M. Halder, M. Wagner, C. Franz, C. Pfleiderer, K. Everschor, M. Garst, and A. Rosch, Emergent electrodynamics of skyrmions in a chiral magnet, Nature Phys. **8**, 301 (2012).

[10] X.Z. Yu, N. Kanazawa, W.Z. Zhang, T. Nagai, T. Hara, K. Kimoto, Y. Matsui, Y. Onose, and Y. Tokura, Skyrmion flow near room temperature in an ultralow current density, Nature Commun. **3**, 988 (2012).

[11] S.-Z. Lin, C. Reichhardt, C.D. Batista, and A. Saxena, Driven skyrmions and dynamical transitions in chiral magnets, Phys. Rev. Lett. **110**, 207202 (2013).

[12] J. Iwasaki, M. Mochizuki, and N. Nagaosa, Universal current-velocity relation of skyrmion motion in chiral magnets, Nature Commun. **4**, 1463 (2013).

[13] D. Liang, J.P. DeGrave, M.J. Stolt, Y. Tokura, and S. Jin, Current-driven dynamics of skyrmions stabilized in MnSi nanowires revealed by topological Hall effect, Nature Commun. **6**, 8217 (2015).

[14] W. Jiang, X. Zhang, G. Yu, W. Zhang, X. Wang, M.B. Jungfleisch, J.E. Pearson, X. Cheng, O. Heinonen, K.L. Wang, Y. Zhou, A. Hoffmann, and S.G.E. te Velthuis, Direct observation of the skyrmion Hall effect, Nature Phys. **13**, 162 (2017).

[15] K. Litzius, I. Lemesh, B. Krüger, P. Bassirian, L. Caretta, K. Richter, F. Büttner, K. Sato, O.A. Tretiakov, J. Förster, R.M. Reeve, M. Weigand, I. Bykova, H. Stoll, G. Schütz, G.S.D. Beach, and M. Kläui, Skyrmion Hall effect revealed by direct time-resolved X-ray microscopy, Nature Phys. **13**, 170 (2017).

[16] W. Legrand, D. Maccariello, N. Reyren, K. Garcia, C. Moutafis, C. Moreau-Luchaire, S. Collin, K. Bouzehouane, V. Cros, and A. Fert, Room-temperature current-induced generation and motion of sub-100 nm skyrmions, Nano Lett **17**, 2703 (2017).

[17] A. Fert, V. Cros, and J. Sampaio, Skyrmions on the track, Nature Nanotechnol. **8**, 152 (2013).

[18] N. Ronning, C. Hanneken, M. Menzel, J.E. Bickel, B. Wolter, K. von Bergmann, A. Kubetzka, and R. Wiesendanger, Writing and deleting single magnetic skyrmions, Science **341**, 636 (2013).

[19] W. Kang, Y. Huang, C. Zheng, W. Lv, N. Lei, Y. Zhang, X. Zhang, Y. Zhou and W. Zhao, Voltage controlled magnetic skyrmion motion for racetrack memory, Sci. Rep. **6**, 23164 (2016).

[20] R. Tomasello, E. Martinez, R. Zivieri, L. Torres, M. Carpentieri, and G. Finocchio, A strategy for the design of skyrmion nanotrack memories, Sci. Rep. **4**, 6784 (2014).

[21] D. Prychynenko, M. Sitte, K. Litzius, B. Krüger, G. Burianoff, M. Kläui, J. Sinova, and K. Everschor-Sitte, A magnetic skyrmion as a non-linear resistive element - a potential building block for reservoir computing, arXiv:1702.04298 (unpublished).

[22] D. Pinna, F. Abreu Araujo, J.-V. Kim, V. Cros, D. Querlioz, P. Bessiere, J. Droulez, J. Grollier, Skyrmion gas manipulation for probabilistic computing, arXiv:1701.07750 (unpublished).

[23] S. Bhattacharya and M.J. Higgins, Dynamics of a disordered flux line lattice, Phys. Rev. Lett. **70**, 2617 (1993).

[24] A.C. Marley, M.J. Higgins, and S. Bhattacharya, Flux flow noise and dynamical transitions in a flux line lattice, Phys. Rev. Lett. **74**, 3029 (1995).

[25] U. Yaron, P.L. Gammel, D.A. Huse, R.N. Kleiman, C.S. Oglesby, E. Bucher, B. Batlogg, D.J. Bishop, K. Mortensen, and K.N. Clausen, Structural evidence for a two-step process in the depinning of the superconducting flux-line lattice, Nature (London) **376**, 753 (1995).

[26] M. Hellerqvist, D. Ephron, W. White, M. Beasley, and A. Kapitulnik, Vortex dynamics in two-dimensional amorphous $Mo_{77}Ge_{23}$ films, Phys. Rev. Lett. **76**, 4022 (1996).

[27] F.I.B. Williams, P.A. Wright, R.G. Clark, E.Y. Andrei, G. Deville, D.C. Glattli, O. Probst, B. Etienne, C. Dorin, C.T. Foxon, and J.J. Harris, Conduction threshold and pinning frequency of magnetically induced Wigner solid, Phys. Rev. Lett. **66**, 3285 (1991).

[28] C. Reichhardt, C.J. Olson, N. Grønbech-Jensen, and F. Nori, Moving Wigner glasses and smectics: Dynamics of disordered Wigner crystals, Phys. Rev. Lett. **86**, 4354 (2001).

[29] K. Cooper, J. Eisenstein, L. Pfeiffer, and K. West, Observation of narrow-band noise accompanying the breakdown of insulating states in high Landau levels, Phys. Rev. Lett. **90**, 226803 (2003).

[30] C. Reichhardt and C. J. Olson, Colloidal dynamics on disordered substrates, Phys. Rev. Lett. **89**, 078301 (2002).

[31] A. Pertsinidis and X.-S. Ling, Statics and dynamics of 2D colloidal crystals in a random pinning potential, Phys. Rev. Lett. **100**, 028303 (2008).

[32] A. Sengupta, S. Sengupta, and G.I. Menon, Driven disordered polymorphic solids: Phases and phase transitions, dynamical coexistence and peak effect anomalies, Phys. Rev. B **81**, 144521 (2010).

[33] C. Reichhardt and C.J.O. Reichhardt, Depinning and nonequilibrium dynamic phases of particle assemblies driven over random and ordered substrates: a review, Rep. Prog. Phys. **80**, 026501 (2017).

[34] M. Faleski, M.C. Marchetti, and A.A. Middleton, Vortex dynamics and defects in simulated flux flow, Phys. Rev. B **54**, 12427 (1996).

[35] Y. Fily, E. Olive, N. Di Scala, and J.C. Soret, Critical behavior of plastic depinning of vortex lattices in two dimensions: Molecular dynamics simulations, Phys. Rev. B **82**, 134519 (2010).

[36] A.E. Koshelev and V.M. Vinokur, Dynamic melting of the vortex lattice, Phys. Rev. Lett. **73**, 3580 (1994).

[37] K. Moon, R.T. Scalettar, and G.T. Zimányi, Dynamical phases of driven vortex systems, Phys. Rev. Lett. **77**, 2778 (1996).

[38] C. J. Olson, C. Reichhardt, and F. Nori, Nonequilibrium dynamic phase diagram for vortex lattices, Phys. Rev. Lett. **81**, 3757 (1998).

[39] F. Pardo, F. de la Cruz, P.L. Gammel, E. Bucher, and D.J. Bishop, Observation of smectic and moving-Braggglass phases in flowing vortex lattices, Nature (London) **396**, 348 (1998).

[40] A. Kolton, D. Domínguez, and N. Grønbech-Jensen, Hall noise and transverse freezing in driven vortex lattices, Phys. Rev. Lett. **83**, 3061 (1999).

[41] A.M. Troyanovski, J. Aarts, and P.H. Kes, Collective and plastic vortex motion in superconductors at high flux densities, Nature (London) **399**, 665 (1999).

[42] H. Fangohr, S. Cox, and P. de Groot, Vortex dynamics in two-dimensional systems at high driving forces, Phys. Rev. B **64**, 064505 (2001).

[43] T.J. Bullard, J. Das, G.L. Daquila, and U.C. Täuber, Vortex washboard voltage noise in type-II superconductors, Eur. Phys. J. B **65**, 469 (2008).

[44] Y. Togawa, R. Abiru, K. Iwaya, H. Kitano, and A. Maeda, Direct observation of the washboard noise of a driven vortex lattice in a high-temperature superconductor, $Bi_2Sr_2CaCu_2Oy$, Phys. Rev. Lett. **85**, 3716 (2000).

[45] A.B. Kolton, D. Domínguez, and N. Grønbech-Jensen, Mode locking in ac-driven vortex lattices with random pinning, Phys. Rev. Lett. **86**, 4112 (2001).

[46] S. Okuma, J. Inoue, and N. Kokubo, Suppression of broadband noise at mode locking in driven vortex matter, Phys. Rev. B **76**, 172503 (2007).

[47] L. Balents, M. C. Marchetti, and L. Radzihovsky, Nonequilibrium steady states of driven periodic media, Phys. Rev. B **57**, 7705 (1998).

[48] T. Giamarchi and P. Le Doussal, Moving glass phase of driven lattices, Phys. Rev. Lett. **76**, 3408 (1996).

[49] A.B. Kolton, R. Exartier, L.F. Cugliandolo, D. Domínguez, and N. Grønbech-Jensen, Effective temperature in driven vortex lattices with random pinning, Phys. Rev. Lett. **89**, 227001 (2002).

[50] J. Müller and A. Rosch, Capturing of a magnetic skyrmion with a hole, Phys. Rev. B **91**, 054410 (2015).

[51] C. Reichhardt, D. Ray, and C.J. Olson Reichhardt, Collective transport properties of driven skyrmions with random disorder, Phys. Rev. Lett. **114**, 217202 (2015).

[52] C. Reichhardt, D. Ray, and C.J. Olson Reichhardt, Quantized transport for a skyrmion moving on a two-dimensional periodic substrate, Phys. Rev. B **91**, 104426 (2015).

[53] C. Reichhardt and C.J.O. Reichhardt, Noise fluctuations and drive dependence of the skyrmion Hall effect in disordered systems, New J. Phys. **18**, 095005 (2016).

[54] J.-V. Kim and M.-W. Yoo, Current-driven skyrmion dynamics in disordered films, Appl. Phys. Lett **110**, 132404 (2017).

[55] S.-Z. Lin, C. Reichhardt, C.D. Batista, and A. Saxena, Particle model for skyrmions in metallic chiral magnets: Dynamics, pinning, and creep, Phys. Rev. B **87**, 214419 (2013).

[56] A. A. Thiele, Steady-state motion of magnetic domains, Phys. Rev. Lett. **30**, 230 (1973).

[57] C. Schütte, J. Iwasaki, A. Rosch, and N. Nagaosa, Inertia, diffusion, and dynamics of a driven skyrmion, Phys. Rev. B **90**, 174434 (2014).

[58] J. Barker and O.A. Tretiakov, Static and dynamical properties of antiferromagnetic skyrmions in the presence of applied current and temperature, Phys. Rev. Lett. **116**, 147203 (2016).